Modified View of Energy Budget Diagram and Its Application to the Kuroshio Extension Region

TAKURO MATSUTA[a] AND YUKIO MASUMOTO[a,b]

[a] *Department of Earth and Planetary Science, Graduate School of Science, The University of Tokyo, Tokyo, Japan*
[b] *Application Laboratory, Japan Agency for Marine-Earth Science and Technology, Yokohama, Japan*

(Manuscript received 8 June 2020, in final form 16 December 2020)

ABSTRACT: The nonlocality of eddy–mean flow interactions, which appears explicitly in the modified Lorentz diagram as a form of the interaction energy, and its link to other estimation methods are revisited, and a new formulation for the potential enstrophy is proposed. The application of these methods to the Kuroshio Extension region suggests that the combined use of energy analysis with other methods, including the potential enstrophy diagram, provides more comprehensive understandings for the eddy–mean flow interactions in the limited region. It is shown that the interaction energy is transported from the nearshore and upstream regions to the downstream region in the form of the interaction energy flux, causing acceleration of the Kuroshio Extension jet in the downstream region. The potential enstrophy diagram indicates that the eddy field decelerates (accelerates) the jet in the nearshore (downstream) region, which is a consistent result with the energy analysis. It turns out that the interaction potential enstrophy flux is radiated from a region of the eddy kinetic energy maximum toward the upstream region, which is the opposite direction from the interaction energy flux. The interaction potential enstrophy flux that originated from this eddy kinetic energy maximum region also convergences near the center of the northern recirculation gyre of the Kuroshio Extension region and tends to stabilize the structures of the recirculation gyre. Together with the energy analysis that indicates the eddy field accelerates the northeastern part of the recirculation gyre through the local interactions, the present analyses support the arguments on the eddy-driven northern recirculation gyre.

KEYWORDS: Eddies; Energy transport

1. Introduction

Interaction between mean flow and eddy perturbations is one of the key issues in physical oceanography, particularly in and around the western boundary currents (WBC) such as the Kuroshio and the Gulf Stream, where strong currents and large eddy activities are often observed (e.g., Chelton et al. 2011). While eddy perturbations are usually considered as a source of dissipation of the mean flow, they sometimes function instead as a driving force for the mean flow. There have been many attempts to investigate the dynamics of strong jets associated with the WBC and their relations to eddy kinetic energy (EKE) and eddy structures (e.g., Qiu et al. 2008; Waterman and Jayne 2011). These studies show, for example, that a recirculation gyre of the WBC is induced through divergence of the Reynolds stress due to eddy perturbations near strong WBC jets and that eddy vorticity forcing changes mean potential vorticity (PV) fields and generates recirculation gyres to the north and south of the WBC jets. Also, quasi-stationary meanders of the WBC jets are considered to be related to eddy–mean flow interactions (e.g., Qiu and Chen 2010).

The Lorentz diagram (Lorentz 1955) is a powerful diagnostic tool for studying such eddy–mean flow interactions and has been widely utilized to show energy budgets in the ocean in previous studies (e.g., Ogata and Masumoto 2011; Magalhães et al. 2017; Wang et al. 2017). The diagram focuses on energy conversion rates among mean kinetic energy, mean available potential energy, EKE, and eddy available potential energy, with quantitative assessment of barotropic and baroclinic instabilities. A remarkable advantage of this diagram and the associated energy estimate formulae is their simplicity, yielding straightforward implementation of the formulae for an analysis of outputs from ocean general circulation models (OGCMs).

The Lorentz diagram, however, is originally intended to be used for global mean condition. An application of this method to a regional analysis and/or discussions on spatial distribution of the energy conversion rates may create misunderstandings regarding the energy flow (Plumb 1983). One example is that the barotropic energy conversion rates in the Lorentz diagram could indicate a large value even without any local instability processes due to energy fluxes from other areas. Therefore, the energy conversion rates in the Lorentz diagram are inadequate in some cases for estimation of eddy–mean flow interactions in a limited region.

Alternative methods based on the wave activity or the pseudo-momentum have been proposed to overcome the above issue in the atmospheric literature (e.g., Andrews 1983; Plumb 1985a,b, 1986; Takaya and Nakamura 2001). However, the assumptions adopted to develop the alternative methods are inapplicable in many cases to a region near the oceanic WBC jets, in which background potential vorticity changes their magnitude abruptly along their stream lines (e.g., Waterman and Jayne 2011). Furthermore, estimation of the wave activity requires rather complicated calculations when

Denotes content that is immediately available upon publication as open access.

Corresponding author: Takuro Matsuta, matsuta@eps.s.u-tokyo.ac.jp

DOI: 10.1175/JPO-D-20-0124.1

using outputs from OGCMs or atmospheric general circulation models in some cases. For these reasons, the Lorentz diagram is widely used in the analysis of oceanic energetics.

Another approach proposed by Murakami (2011) and Chen et al. (2014, 2016) is to modify the energy conversion rates in the Lorentz diagram for a local estimation. This approach allows us to estimate locally induced energy transfer between mean flow and eddy perturbations explicitly, as well as the effects of "nonlocal" energy fluxes (Chen et al. 2014, 2016). Murakami (2011) further examines the relationship between these modified energy transfers and wave activity and indicates that the modified Lorentz diagram can capture eddy–mean flow interactions in a way that is consistent with other related methods. However, since physical interpretations of the nonlocal energy fluxes are not given explicitly and horizontal distributions of the nonlocal energy fluxes and their link to mean structures of flow fields in an oceanographic context have not been analyzed yet in detail, our understanding of energetics in a regional area is still limited, and further investigation is required.

There are several possible ways as described above to examine the transfer of energy between mean flow and eddy perturbations. In the present study, we first review energy conversion rates and related terms in the modified Lorentz diagram. We extend our arguments to potential enstrophy, which is another conservative quantity for a water parcel, to obtain a complementary view to the energy diagram. The Lorentz-type diagram in terms of the potential enstrophy and its relation to the nonlocality of eddy–mean flow interactions are documented for the first time in this study. Then, we apply the modified Lorentz diagram to a region in the Kuroshio Extension (KE) region. Our particular focus here is to discuss physical interpretations of the interaction energy flux and equivalent fluxes in related expressions and to show their distributions in the KE region. As an example of the advantage of combining several viewpoints of the energy diagram, we will briefly discuss the dynamics of the KE recirculation gyres.

In general, both the baroclinic and barotropic processes are important in the WBC jet regions. However, to highlight the above points in a clear and concise way, we only focus on barotropic processes in the energy analysis in the present study. More complete descriptions of a total view of energetics in the KE region is beyond the scope of this paper. Note that baroclinic processes can be treated in the same manner as that for barotropic processes demonstrated in this article, and baroclinic effects are also included in the case of potential enstrophy conversion rates.

This paper is organized as follows. Brief descriptions for each method are shown with their physical interpretations in section 2. Section 3 compares energy conversion rates between the classical Lorentz diagram and the modified diagram in the KE region as a key example. Also, the potential enstrophy conversion rates are discussed. Section 4 shows the analysis of energy and potential enstrophy for the KE northern recirculation gyre and demonstrates the nonlocality of the eddy–mean flow interactions. Finally, section 5 provides a summary of this paper.

2. Lorentz diagram and the modified energy and potential enstrophy transfer diagram

a. Modified energy conversion rates

We consider a variable x that can be described by its time-mean value $\overline{x}$, and eddy perturbations x' as a deviation from the mean, i.e.,

$$x' = x - \overline{x}. \tag{1}$$

With this separation between the mean field and eddy perturbations, the barotropic energy conversion rate (BTR) in the classical Lorentz diagram is given as follows (Lorentz 1955):

$$\mathrm{BTR} = -\rho_0(\overline{u'\mathbf{u}'}\cdot\nabla\overline{u} + \overline{v'\mathbf{u}'}\cdot\nabla\overline{v}), \tag{2}$$

where ρ_0 is the constant reference density; $\mathbf{u}$ is the velocity, with u and v as the zonal and meridional components; and ∇ is the three-dimensional gradient operator. This BTR is the product of the gradient of the mean flow and eddy Reynolds stresses, and a positive BTR value denotes energy gain in EKE through eddy–mean flow interactions. The BTR is considered to be the energy released from the mean kinetic energy in the classical Lorentz diagram.

On the other hand, the modified energy transfer terms for the barotropic processes proposed by Murakami (2011) and Chen et al. (2014, 2016) have two expressions. According to Chen et al. (2014), kinetic energy equations can be expressed as follows:

$$\frac{\partial}{\partial t}K_M + \nabla\cdot(\overline{\mathbf{u}}\cdot K_M) + \nabla\cdot(\overline{\mathbf{u}}\,\overline{p}) = -g\overline{\rho}\,\overline{w} - M_{K_M} + X_{K_M}, \tag{3}$$

$$\frac{\partial}{\partial t}K_E + \nabla\cdot\left[\overline{\mathbf{u}\frac{1}{2}\rho_0(u'^2+v'^2)}\right] + \nabla\cdot(\overline{\mathbf{u}'p'}) = -g\overline{\rho'w'} + M_{K_E} + X_{K_E}, \tag{4}$$

where $K_M = (1/2)\rho_0(\overline{u}^2+\overline{v}^2)$ is the kinetic energy of the mean flow; K_E is the EKE; and X_{K_M} (X_{K_E}) is the rate of change of K_M (K_E) due to friction, wind stress, and bottom drag. Here, M_{K_M} denotes the rate of change of the mean kinetic energy due to eddy momentum flux, while M_{K_E} is the rate of change of the eddy kinetic energy due to eddy momentum flux, which is the same as the BTR. These terms can be written as

$$M_{K_M} = \rho_0(\overline{u}\nabla\overline{u'\mathbf{u}'} + \overline{v}\nabla\overline{v'\mathbf{u}'}) \approx \rho_0(\overline{u}\nabla_h\overline{u'\mathbf{u}'_h} + \overline{v}\nabla_h\overline{v'\mathbf{u}'_h}), \tag{5}$$

$$M_{K_E} = \mathrm{BTR} = -\rho_0(\overline{u'\mathbf{u}'}\cdot\nabla\overline{u} + \overline{v'\mathbf{u}'}\cdot\nabla\overline{v}) \approx -\rho_0(\overline{u'\mathbf{u}'_h}\cdot\nabla_h\overline{u} + \overline{v'\mathbf{u}'_h}\cdot\nabla_h\overline{v}), \tag{6}$$

where $\mathbf{u}_h$ is the horizontal velocity and ∇_h is the horizontal gradient operator. Since the vertical terms in the energy conversion rates, such as $-\overline{u'w'}(\partial/\partial z)\overline{u}$, are small compared to the other horizontal terms, we neglect them in the following analyses.

The difference between the two terms, $M_{K_I} = M_{K_M} - M_{K_E}$, can be expressed as

$$M_{K_I} = \rho_0\nabla_h\cdot(\overline{u}\,\overline{u'\mathbf{u}'_h} + \overline{v}\,\overline{v'\mathbf{u}'_h}) = \rho_0\nabla_h\cdot\overline{\mathbf{u}_h(\overline{u}u' + \overline{v}v')}. \tag{7}$$

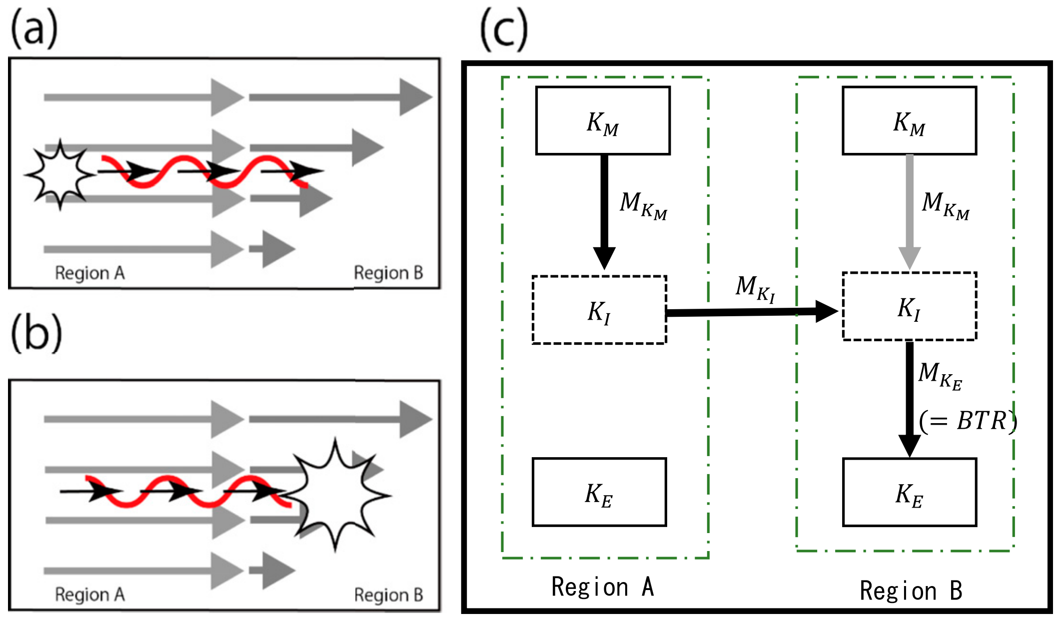

FIG. 1. Schematic diagrams showing horizontal distributions of mean flow and processes associated with eddy–mean flow interactions in an idealized situation, (a) when interaction energy represented by the red wavy line is generated from the mean flow in the upstream region (region A; the left half of each panel) and (b) when interaction energy is used to generate eddy perturbations in the downstream region (region B; the right half of each panel). The gray arrows in (a) and (b) indicate background flows, with no horizontal shear of zonal flow in region A and with positive meridional shear in region B. The condition of barotropic instability is assumed to be satisfied only in region B. (c) The modified energy diagrams for regions A and B in the above idealized case. The interaction energy K_I is transported out by the homogeneous background flow from region A [indicated as black arrows in (a)]. Associated disturbances transported into region B interact with the mean shear flow, causing the disturbances to grow via barotropic conversion, i.e., the interaction energy together with M_{K_M} in region B is converted into K_E.

Since this difference is an advection of interaction energy $K_I = (\overline{u}u' + \overline{v}v')$ defined in Murakami (2011), an integral of this term over the global domain vanishes, resulting in $M_{K_M} = M_{K_E} =$ BTR. Therefore, the modified energy budget becomes identical to the classical view in the global mean condition.

However, this is not the case for an energy diagram in a limited domain, which is frequently used in the oceanographic literature. The difference term, M_{K_I}, may have a nonzero value in such a case and plays an important role in energy transfer between the mean flow and eddy perturbations. For $M_{K_M} \approx$ BTR, the energy conversion through the barotropic instability occurs locally, i.e., energy is transformed from mean kinetic energy to EKE within a target region. In this case, the classical Lorentz diagram and an associated barotropic energy conversion rate correctly represent the eddy–mean flow interaction even for a limited domain. However, in the case of $M_{K_M} \neq$ BTR, a part of the energy is transported to or from the other areas outside of the target region by the difference term, which is called the nonlocal interaction in Chen et al. (2014, 2016). Although this interaction energy K_I vanishes in the time mean, its flux does not. Horizontal distribution of the kinetic energy is therefore affected by this energy flux, which is not evaluated explicitly in the classical Lorentz diagram.

The interaction energy flux can be considered as seeds of instability in some cases, as illustrated in Fig. 1. There are two regions located face-to-face with different background velocity fields (Fig. 1a); a uniform zonal current can be seen in region A, and zonal currents with meridional shear that allows barotropic instability in region B. Consider a case in which a small disturbance appears in region A. Since the necessary condition for barotropic instability is not satisfied in region A, the EKE there does not grow, i.e., BTR = 0. On the other hand, M_{K_M} can be generated if Reynolds stress associated with the disturbance is spatially nonuniform. The difference between the two, i.e., energy corresponding to M_{K_M}, is transported out from region A as the flux of the interaction energy M_{K_I} into region B. It is this energy flux that can be considered the seeds of the BTR, by which the interaction energy is converted to the EKE via the background field that provides the unstable condition in region B (Fig. 1b). The corresponding modified energy diagram for this particular case is shown in Fig. 1c. In region B, K_I transported from region A interacts with the mean shear flow to initiate barotropic energy conversion, which requires M_{K_M} (shown as a gray arrow in Fig. 1c) to extract energy from the mean flow to eddy disturbances, if the BTR appears. However, in reality, local barotropic instability can occur alongside any other disturbance within region B, and the energy conversions are more complicated.

b. *Enstrophy budget*

An eddy–mean flow interaction diagram for the potential enstrophy can be obtained in the same way as that for the modified Lorentz diagram. For quasigeostrophic oceanic motions, the quasigeostrophic potential vorticity (QGPV) q is defined by

$$q = (f - f_0) + \zeta + f_0 \frac{\frac{\partial \sigma}{\partial z}}{\frac{\partial \langle \sigma \rangle}{\partial z}}, \tag{8}$$

where ζ denotes the relative vorticity, f is the Coriolis parameter, f_0 is the Coriolis parameter averaged in the target region, σ is the potential density, and $\langle \sigma \rangle$ is the potential density averaged over time and space (Nakamura and Chao 2001; Qiu et al. 2008). This definition of QGPV was previously used to investigate the Kuroshio northern recirculation gyre generation mechanism by Qiu et al. (2008). By neglecting the external forcing and subgrid dissipation, the potential enstrophy equation for mean flow and eddy perturbation can be obtained as below:

$$\frac{\partial}{\partial t} e_M + \nabla_h \cdot (\overline{\mathbf{u}} \cdot e_M) = -M_{e_M}, \tag{9}$$

$$\frac{\partial}{\partial t} e_E + \nabla_h \cdot (\overline{\mathbf{u}} \cdot e_E) = M_{e_E}, \tag{10}$$

where $e_M = (1/2)\overline{q}^2$ denotes the mean potential enstrophy, $e_E = (1/2)\overline{q'q'}$ is the eddy potential enstrophy, $M_{e_M} = \overline{q}\nabla_h \cdot (\overline{\mathbf{u}'q'})$ is the rate of change of mean potential enstrophy due to eddy QGPV fluxes, and $M_{e_E} = -\overline{\mathbf{u}'q'} \cdot \nabla_h \overline{q}$ is the rate of change of eddy potential enstrophy due to eddy QGPV fluxes. A cascade type diagram of the enstrophy conversion can be drawn using the Eqs. (9) and (10) (Fig. 2). In the diagram, the mean flow loses its potential enstrophy at the rate of M_{e_M}, some of which is converted to e_E through M_{e_E}, and the residual $M_{e_I} = M_{e_M} - M_{e_E}$ should be transported out to other regions. Since M_{e_I} is equal to $\nabla_h(\overline{q}\,\overline{\mathbf{u}'q'})$, we call this term the "interaction potential enstrophy flux." Adding (9) to (10), the total potential enstrophy equation is obtained as

$$\frac{\partial}{\partial t}(e_M + e_E) + \nabla_h \cdot [\overline{\mathbf{u}} \cdot (e_M + e_E)] = -M_{e_I}, \tag{11}$$

indicating that the interaction potential enstrophy flux M_{e_I} is the total enstrophy radiation through eddy–mean flow interactions. Note that the interaction energy flux M_{K_I} discussed in section 2a is also considered as the transport of total kinetic energy in the same manner (see the appendix for more detailed discussions).

It is worth mentioning that the mean potential vorticity can be shifted by constant values while keeping the resultant quasigeostrophic flow unchanged. On the other hand, this constant shift changes the mean potential enstrophy e_M. When q is shifted by an arbitrary constant value f_c, the corresponding Eq. (11) should be modified as

$$\left\{\frac{\partial}{\partial t}(e_M + e_E) + \nabla_h \cdot [\overline{\mathbf{u}} \cdot (e_M + e_E)]\right\} + f_c\left[\frac{\partial}{\partial t}\overline{q} + \nabla_h \cdot (\overline{\mathbf{u}}\,\overline{q}) + \nabla_h \cdot \overline{(\mathbf{u}'q')}\right] = -M_{e_I}. \tag{11$'$}$$

The difference between (11) and (11′) leads to

$$\frac{\partial}{\partial t}\overline{q} + \nabla_h \cdot (\overline{\mathbf{u}}\,\overline{q}) + \nabla_h \cdot (\overline{\mathbf{u}'q'}) = 0, \tag{12}$$

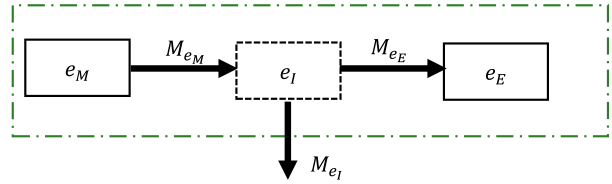

FIG. 2. A schematic diagram indicating the enstrophy transfer through eddy–mean flow interactions. Other elements such as advection are omitted. The mean flow loses its potential enstrophy corresponding to M_{e_M}, some of which is converted into eddy disturbances by M_{e_E} while the rest is transported out to other regions by M_{e_I}.

which is the mean potential vorticity equation. Since the third term of the Eq. (12) is derived from the interaction potential enstrophy flux term, M_{e_I} may correspond to the eddy vorticity flux divergence in the potential enstrophy budget.

3. Interpretations of energy and potential enstrophy budget in the Kuroshio Extension region

a. Data and basic structures of the KE jet

To demonstrate the differences in the energy transfer terms in the classical and modified Lorentz diagrams and their interpretations, results from an eddy-resolving OGCM named OGCM for the Earth Simulator (OFES) (Masumoto et al. 2004), are used in the following analyses. OFES is based on the Modular Ocean Model version 3 (MOM3) developed at GFDL (Pacanowski and Griffies 2000) and optimized for the massively parallel computational architecture of the Earth Simulator. The horizontal grid spacing is 0.1° × 0.1°, and there are 54 vertical levels. The 3-day, NCEP-run snapshots from 1993 to 2012, which are forced by NCEP reanalysis products, are used [see Sasaki et al. (2006, 2008) for more detailed model settings]. It has been shown that OFES captures large-scale circulations as well as mesoscale eddies realistically (e.g., Masumoto et al. 2004; Sasaki et al. 2008; Masumoto 2010, and references therein), providing a reasonable platform to examine the eddy–mean flow interactions discussed in the previous section. We consider, for the following analyses, time averaged values to be background mean conditions, and deviations from them are defined as eddy perturbations.

Horizontal distributions of the mean EKE and sea surface elevation averaged from 1993 to 2012 calculated from the OFES results are shown for the KE region in Fig. 3. The KE is represented as the strong eastward meandering jet, whose volume transport per unit width integrated in the depth exceeds 200 $\mathrm{m^2\,s^{-1}}$. In the region west of 150°E, the EKE has large values along the stationary meandering Kuroshio jet. After the EKE indicates its maximum around 153°E, the zonal jet is stabilized in the region east of 155°E. The jet broadens around 155°E, and northern and southern edges of the jet tend to turn back westward in a region north and south of the jet, respectively. The southern recirculation gyre (SRG), with the anticyclonic circulation and associated higher sea surface height (SSH), occupies the region 32°–34°N, 140°–155°E (Fig. 3b). The cyclonic northern recirculation gyre (NRG) can be seen in the region 35°–38°N, 145°–153°E, but the westward flow in the

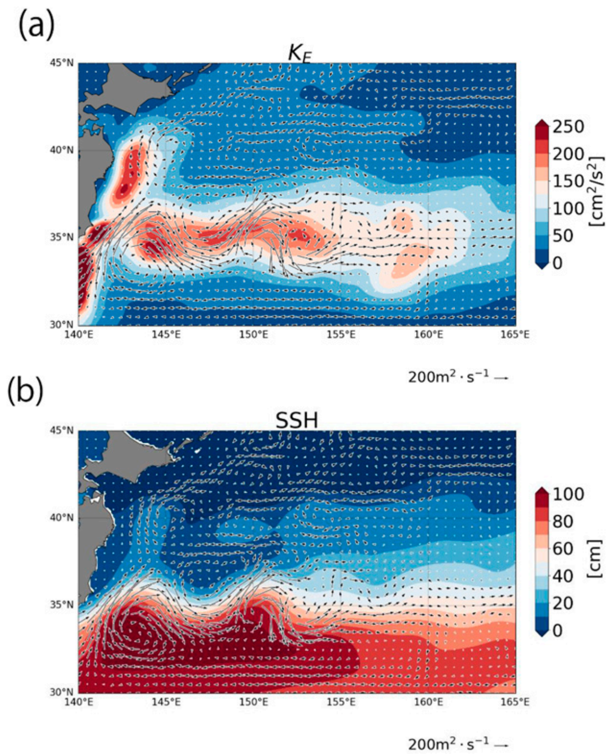

FIG. 3. Horizontal distribution of (a) the EKE and (b) the mean sea surface elevation obtained from the OFES results for the period of 1993–2011. The EKE is integrated from the ocean surface to the ocean bottom. Black arrows represent horizontal volume transport per unit width integrated through the water column.

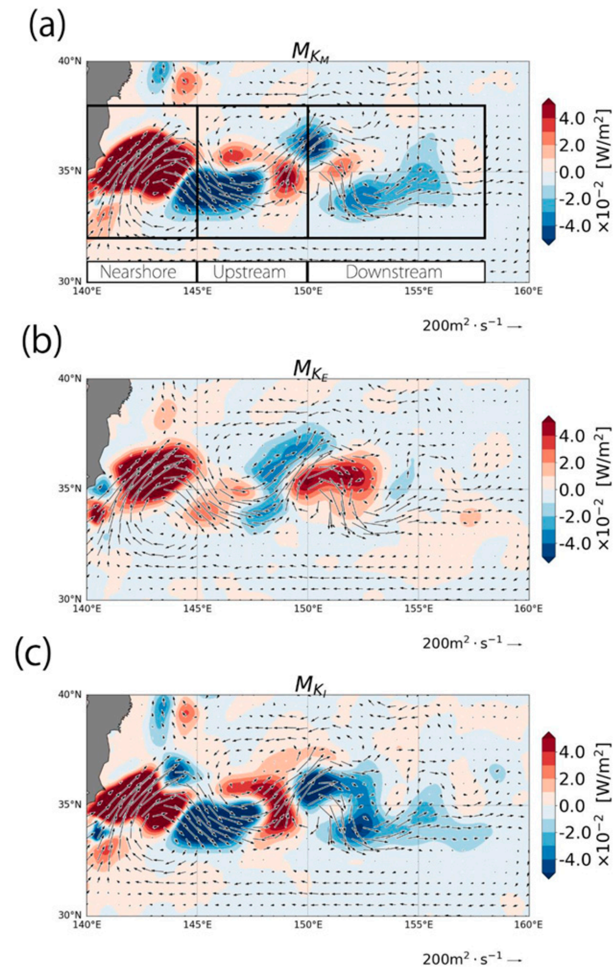

FIG. 4. Horizontal distributions of (a) M_{K_M}, (b) M_{K_E}, and (c) M_{K_I}. Superposed black arrows show the mass transport per unit width of the mean flow integrated from the ocean surface to the ocean bottom. The three black boxes in (a) represent the nearshore (140°–145°E), upstream (145°–150°E), and downstream (150°–158°E) regions, in the latitude band of 32°–38°N used in the later analyses.

northern part is weaker and the lower SSH is less visible compared to the SRG (Qiu et al. 2008; Aoki et al. 2016). All these characteristics of the KE jet and the associated recirculation structures are consistent with previous results (e.g., Qiu et al. 2008; Qiu and Chen 2010, and references therein).

b. *Energy conversion rates*

Figure 4 shows spatial distributions of the three terms discussed in section 2 for the energy diagram, i.e., M_{K_M}, M_{K_E}, and M_{K_I}. These energy conversion rates are integrated from the sea surface down to the bottom through the water column. We have confirmed, however, that results are almost the same if we integrate only in the upper 600 m where the strong jet and associated eddy signals are confined. Figures in this subsection are drawn with a spatial average over 0.5° × 0.5° boxes to reduce small-scale noise.

Both M_{K_M} and M_{K_E} along the KE jet show large positive values in the nearshore region (140°–145°E), while M_{K_M} shows mostly negative values in the region east of 150°E (hereafter called the downstream region). In between, alternating positive and negative values can be seen in the region between 145° and 150°E (hereafter, the upstream region). Figure 5 indicates the area-integrated M_{K_M} and M_{K_E}, together with M_{K_I}, in each region to show the above tendency clearly. Integration in the meridional direction is taken for the latitude band between 32° and 38°N. In the nearshore region, the area-integrated M_{K_M} shows a large positive value of 12.2×10^9 W, suggesting the mean Kuroshio jet releases a large amount of its energy to the eddy field. However, the magnitude of M_{K_E} in the nearshore region is 6.53×10^9 W, which is 54% of the M_{K_M} value, with some negative regions (Fig. 4b). This indicates that some part of the energy released by the mean Kuroshio jet is transported outward from the nearshore region instead of locally transferred to the perturbation field within the region.

On the other hand, the area integrated M_{K_M} in the downstream region reaches -4.00×10^9 W, while the area-integrated M_{K_E} is 1.57×10^9 W, which is positive. This indicates that the eddy perturbations cannot locally supply the kinetic energy for the mean flow, suggesting another energy source exists for M_{K_M}.

The above discrepancies between M_{K_M} and M_{K_E} correspond to divergence or convergence of the interaction energy flux M_{K_I} (Fig. 4c). In the nearshore region, M_{K_I} shows a large

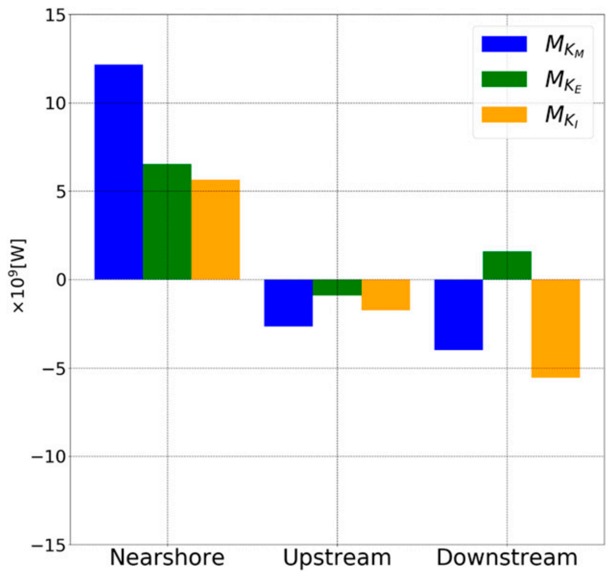

FIG. 5. Area- and depth-integrated M_{K_M}, M_{K_E}, and M_{K_I} in the nearshore, upstream, and downstream shown in Fig. 4a. Depth integration is conducted through the water column.

positive value, suggesting the release of the interaction energy from the region. On the other hand, it tends to have negative values in the downstream region, corresponding to an accumulation of the interaction energy there. The interaction energy generated in the nearshore region through eddy–mean flow interactions is advected eastward into the upstream region in the form of M_{K_I}, and the interaction energy advected from the upstream region to the downstream region is transferred to enhance the mean Kuroshio jet in the downstream region. This is the reason why M_{K_M} has relatively large negative values without local barotropic energy conversions. Since the classical Lorentz diagram depicts the local energy gained by or released from the eddy perturbations, the energy transfer as viewed from the mean flow differs from it by an amount equal to M_{K_I}.

In the upstream region between 145° and 150°E, the important role played by the interaction energy flux in the modified energy diagram can also be seen, but within relatively small regions. For example, the mean flow acceleration around 145°E is located mainly in the region of positive M_{K_E}, suggesting that remotely supplied energy is responsible there. Consulting the M_{K_I} distributions in Fig. 4c, the interaction energy diverges from the nearshore region and converges at around 145°E. It is likely that the energy source of the mean flow acceleration at 145°E is located in the nearshore region.

The above examples clearly demonstrate that the arguments solely based on the barotropic energy conversion rates, as in discussions based on the classical diagram, may result in misinterpreting energy relations in a limited region. For a more accurate understanding of the eddy–mean flow interactions, we should consider M_{K_M} and M_{K_E} from two viewpoints and the nonlocal interaction represented by M_{K_I}, and connect the two conversion terms as formulated by Murakami (2011) and Chen et al. (2014).

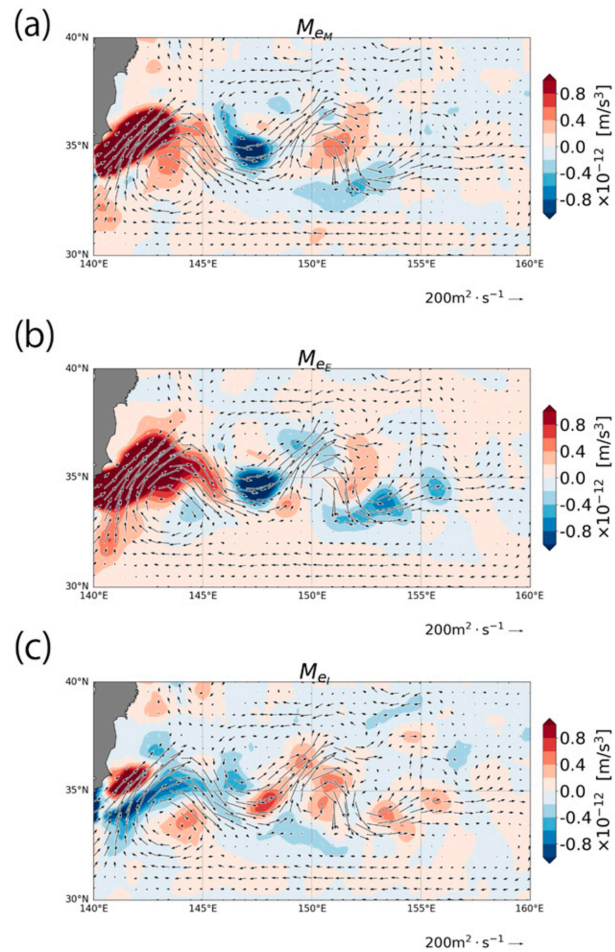

FIG. 6. As in Fig. 4, but for (a) M_{e_M}, (b) M_{e_E}, and (c) M_{e_I}.

c. Potential enstrophy conversion rates

The potential enstrophy conversion rates shown in Fig. 6 provide a complementary view for the energy analysis. While M_{e_E} and M_{e_M} show similar spatial distributions, there are some differences between the two conversion rates, which is shown as M_{e_I} in Fig. 6c. In the nearshore region, M_{e_M} has rather large positive values, indicating a reduction of the potential enstrophy in the mean flow. The area integrated M_{e_E} over the nearshore region is 0.24 $m^3 s^{-3}$, of which 88% is due to the local mean potential enstrophy loss through M_{e_M}. The remaining 12%, i.e., 0.03 $m^3 s^{-3}$, is supplied from the convergence of the interaction potential enstrophy flux. On the other hand, both M_{e_M} and M_{e_E} show negative values in the region east of 145°E, suggesting that the eddy–mean flow interactions tend to stabilize the mean flow, except for a region of weak positive values around 150°E, where the mean flow bifurcates. Therefore, the potential enstrophy budget also suggests mean flow deceleration (acceleration) in the nearshore (downstream) region, which is consistent with the energy analysis. On the other hand, in the region between 145° and 150°E, the enstrophy budget indicates mean flow stabilization due to eddy forcing. This difference from the energy analysis suggests that the combination of several viewpoints is necessary to reveal detailed processes of eddy–mean flow interactions, an example of which will be shown in the next section.

It should be noted here that the direction of the interaction potential enstrophy transport is opposite to that of the interaction energy flux. The interaction potential enstrophy flux integrated between 150° and 165°E (including both the upstream and downstream regions) is 0.01 $m^3 s^{-3}$, suggesting that the total potential enstrophy is transported from the upstream/downstream region to the nearshore region. This may be of relevance to the wave maker mechanism suggested by previous studies (Rhines and Holland 1979; Waterman and Jayne 2011; Waterman and Hoskins 2013), in which the eddies radiate Rossby waves toward the upstream region. This process may be reflected in the direction of the interaction enstrophy flux and also related to the direction of the wave activity flux, which is parallel to the direction of wave propagation in the barotropic plane wave case.

4. Application to the northern recirculation gyre

The NRG may be one of the best phenomena for which arguments based on the energy and potential enstrophy conversion rates can be applied to better understand its dynamics. It has been shown that the NRG spans from east of the Japan Trench at around 145°E, to around 156°E west of the Shatsky Rise, and is confined to the north by the subarctic boundary along 40°N within the depth range from 600 m to around 1500 m (e.g., Qiu et al. 2008) (Fig. 7a). Qiu et al. (2008) suggested that the NRG was driven by the convergence of the Reynolds stress, which accelerates the westward mean flow north of the Kuroshio jet, particularly in the eastern part of the NRG. Their potential vorticity budget also indicated a possibility of the eddy-driven NRG. In addition, they investigated a model based on the turbulent Sverdrup equation by eddy PV forcing, $-\nabla \cdot (\overline{\mathbf{u}'q'})$, obtained from the outputs of another high-resolution model, and successfully reproduced a realistic NRG.

In this section, we revisit NRG dynamics from the viewpoints of energy conversion rates and potential enstrophy conversion rates. To highlight the NRG characteristics, we analyze horizontal distributions of various parameters at a depth of 1342 m. This choice of depth is arbitrary, as we have confirmed that the spatial structure for each conversion rate is essentially the same between depths of 1000 and 1500 m.

a. Energy-based analysis

The horizontal distributions of the EKE magnitude and Reynolds stress near the recirculation gyres are shown in Fig. 7. Large EKE is confined in a latitude band of the meandering jet and the EKE maximum is located around the bifurcation point of the jet at 152°E. A relatively small secondary maximum can be seen at 37°N, 154°E, to the west of the Shatsky Rise. The zonal component of the Reynolds stress (Fig. 7b) shows that the Kuroshio jet is decelerated (accelerated) by eddy forcing in the nearshore (upstream) region. After a part of the Kuroshio jet bifurcates to the north in the downstream region around 152°E, the southern branch seems to be accelerated

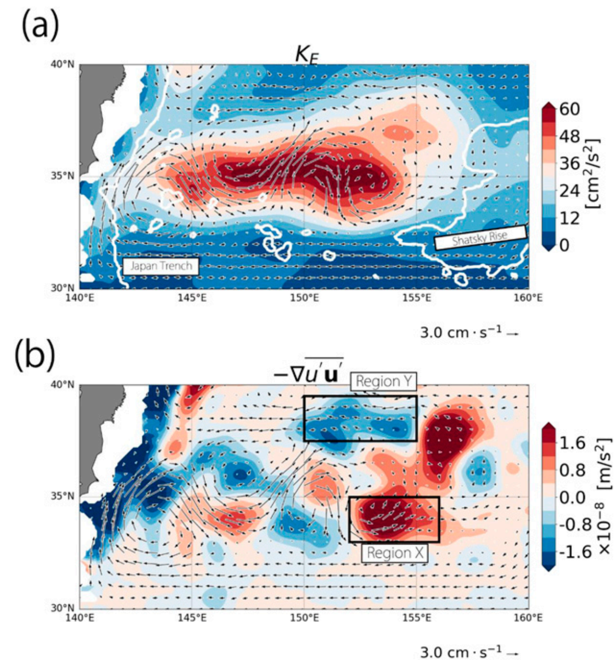

FIG. 7. Horizontal distributions of (a) the EKE and (b) zonal component of the Reynolds stress at a depth of 1342 m. Positive values in (b) correspond to eastward forcing. The black arrows indicate horizontal velocities at a depth of 1342 m. The white contours in (a) indicate the 5000-m isobath. The region surrounded by this contour to the east of 155°E corresponds to the Shatsky Rise. The Japan Trench off the Japan archipelago is also represented by the 5000-m isobath. The zonal eddy forcing accelerates the mean flow in both region X and region Y.

by a convergence of the zonal Reynolds stress (region X in Fig. 7b), while a divergence of the zonal Reynolds stress is observed in the region around 37.5°–39.5°N, 150°–155°E (region Y in Fig. 7b) for the northern branch of bifurcated jet, which turns westward within the region. The northern branch of the bifurcated jet joins the westward flow centered at 39°N and results in the formation of the eastern part of NRG. This is reflected in the M_{K_M} distribution by a negative minimum at the same location (Fig. 8a), suggesting that the NRG generation can be explained by the energy conversion rates (see region Y in Fig. 8a) as well as by the Reynolds stress. In addition, the eddy acceleration of the southern branch of the jet is also captured in M_{K_M} with a negative minimum centered at 33°N, 152°E (see region X in Fig. 8a).

The analysis of energy conversion rates also suggests the importance of the nonlocal eddy–mean flow interactions. In particular, M_{K_I} plays a role in generating the structure of NRG together with the local eddy–mean flow interaction indicated by M_{K_E} (Fig. 8b). Although the local eddy–mean flow interaction mainly accelerates the mean westward flow in region Y, positive M_{K_E} values are also observed at around 38°N, 154°E. This mean flow energy loss is canceled out by the interaction energy flux convergence, as seen below.

The horizontal distributions of M_{K_I} (Fig. 8c) indicate that there is a region of the interaction energy flux convergence

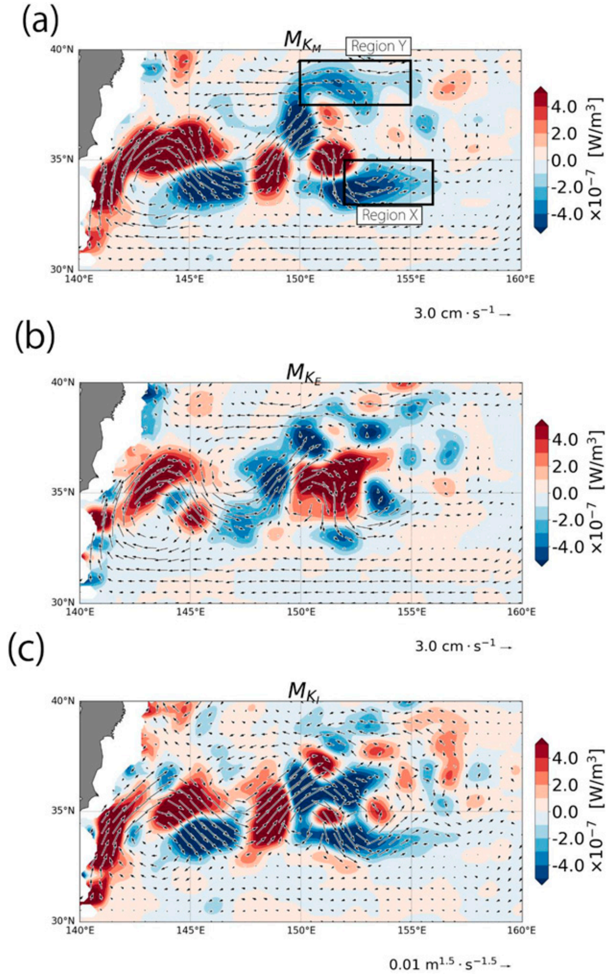

FIG. 8. Horizontal distributions of (a) M_{K_M}, (b) M_{K_E}, and (c) M_{K_I} near the recirculation regions at a depth of 1342 m. Positive values represent the loss of the mean kinetic energy, the gain of the EKE, and the divergence of the interaction energy flux, respectively. Black arrows in (a) and (b) show horizontal velocities at a depth of 1342 m, while those in (c) indicate the interaction energy flux. Note that length of the black arrows in (c) is drawn to be proportional to the square root of the interaction energy flux amplitude to clearly illustrate weaker fluxes. Region X and region Y in (a) are the same regions as in Fig. 7b.

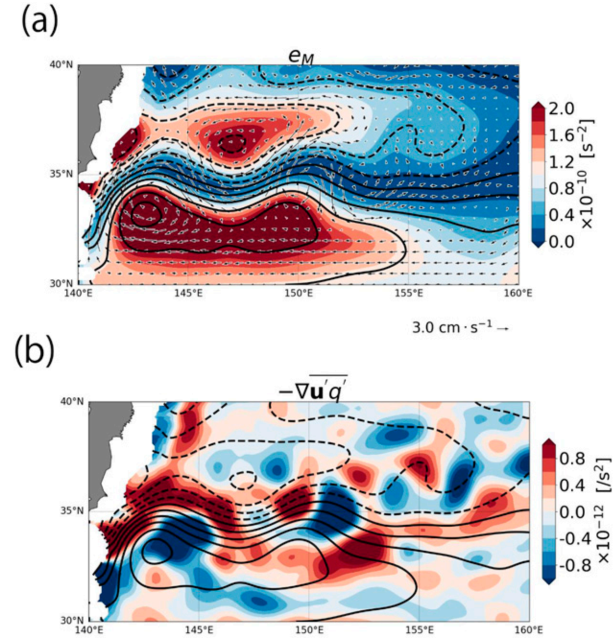

FIG. 9. Horizontal distributions of (a) the mean potential enstrophy and (b) the convergence of the QGPV flux at a depth of 1342 m in color shades. Black contours in (a) and (b) represent the QGPV with a contour interval of $0.5 \times 10^{-5}\,\mathrm{s}^{-1}$. Dashed contours indicate negative QGPV values. Black arrows in (a) show horizontal velocities at 1342-m depth.

between 38°N, 150°E and 40°N, 154°E. This area corresponds to the region where the northward bifurcated flow joins the westward flow to form the cyclonic circulation of the eastern part of the NRG (Fig. 8a). The interaction flux vectors over this area point westward and can be traced back to the east to a region of interaction energy flux divergence around 157°E, just northwest of the Shatsky Rise. This interaction energy, together with M_{K_E}, is converted to mean kinetic energy and accelerates the westward flow in the region of negative M_{K_I}. Thus, the energy analysis can provide additional information about nonlocal effects likely associated with the local topography, which would be difficult to detect only from the momentum viewpoint.

It is worth noting that the westward eddy forcing inside the NRG, indicated by the negative minimum of Reynolds stress convergence, has little effect on the kinetic energy (Figs. 7b and 8a). However, eddy variability also affects horizontal structure around the center of the NRG through the potential enstrophy transport, which will be discussed in the next subsection.

b. *Potential-enstrophy-based analysis*

Horizontal distributions of mean potential enstrophy and convergence of the QGPV flux at 1342-m depth are shown in Fig. 9. The mean QGPV distribution indicated by the black contours in Fig. 9 well reflects the Kuroshio jet and the structures of the recirculation gyres. In the region west of 150°E, the QGPV front exists along the strong Kuroshio jet. The meridional gradients of the QGPV (not shown) change their sign at the flanks of both sides of the jet, satisfying the necessary conditions for an unstable jet. The QGPV contours broaden in the downstream (east of 150°E) region, and the jet becomes stable there as discussed in Waterman and Jayne (2011). On the southern (northern) flank of the jet, there is a positive (negative) maximum of QGPV associated with the southern (northern) recirculation gyre. Reflecting the closed QGPV structures, the mean potential enstrophy distribution has maxima located within the recirculation gyres. Influences of eddy perturbations on the mean flow through the eddy QGPV flux can be identified by comparing the mean QGPV distribution with the convergence of the QGPV fluxes (see Fig. 9b).

In the nearshore region between 142° and 146°E, convergence (divergence) of the QGPV fluxes appears along the northern (southern) half of the Kuroshio jet, indicating that the eddy components tend to weaken the mean QGPV front by increasing (decreasing) the mean QGPV in the northern (southern) region, associated with the unstable nature of the jet. On the other hand, relatively large negative values of the eddy QGPV flux convergence are observed inside the NRG, with large minima located around (37°N, 148°E), (38°N, 154°E), and (36°N, 157°E), and a smaller one at (37°N, 146°E). The divergence of the eddy QGPV flux corresponds to enhancement of the mean potential enstrophy, which supports the suggestion by Qiu et al. (2008) that the NRG could be the eddy driven recirculation. To the south of the Kuroshio jet, large positive values of $-\nabla \cdot (\overline{\mathbf{u}'q'})$ can be seen between 150° and 155°E within the latitude band of 32°–34°N. Contrary to the NRG situation, the location of this maximum is mostly out of phase with the potential enstrophy maximum associated with the SRG, suggesting weaker eddy forcing in the SRG region (Qiu et al. 2008).

The potential enstrophy conversion rates M_{e_M} also well capture the eddy effects on the NRG structure (Fig. 10a). In the nearshore region and the northern half of the jet, M_{e_M} shows positive values, suggesting the mean KE jet releases a large amount of its potential enstrophy to the eddy field. The eddy field, then, enhances the mean flow at the flanks of the jet, shown as regions with negative values in Fig. 10a. As in the case of the mean QGPV analysis, the eddy–mean flow interaction stabilizes the NRG with negative M_{e_M}, while the center of the southern recirculation gyre is misaligned with the negative minimum of M_{e_M}.

Since the mean QGPV is highly homogenized inside the recirculation region, eddy perturbations do not easily grow locally. In fact, the meridional gradient of the mean QGPV does not change its sign in the regions outside of the Kuroshio jet (not shown). While M_{e_M} shows relatively large values outside of the Kuroshio jet, particularly in and near the recirculation gyres, large signals of M_{e_E} are confined along the Kuroshio jet (Fig. 10b). The differences between the two conversion rates are related to the interaction potential enstrophy fluxes, by which the potential enstrophy is transported from one place to another. Figure 10c clearly indicates that the interaction potential enstrophy fluxes that converge within the NRG originate from the divergence region in the Kuroshio jet between 146° and 150°E, where the EKE maximum exists (Fig. 7a). The interaction potential enstrophy flux also radiates from the same region toward the northern part of the SRG, suggesting that the eddy field contributes to stabilizing the SRG to some extent. Note that the interaction potential enstrophy fluxes in the eastern part of NRG can be traced back to the divergence region of the interaction potential enstrophy fluxes in the Kuroshio jet between 153° and 156°E. In the barotropic quasigeostrophic zonal jet case, it has been understood that eddy perturbations radiate eddy QGPV flux outward from the EKE maximum region and generates the NRG and SRG (Waterman and Jayne 2011; Waterman and Hoskins 2013). The same mechanism can be considered to be nonlocal eddy–mean flow interactions in our potential enstrophy analysis.

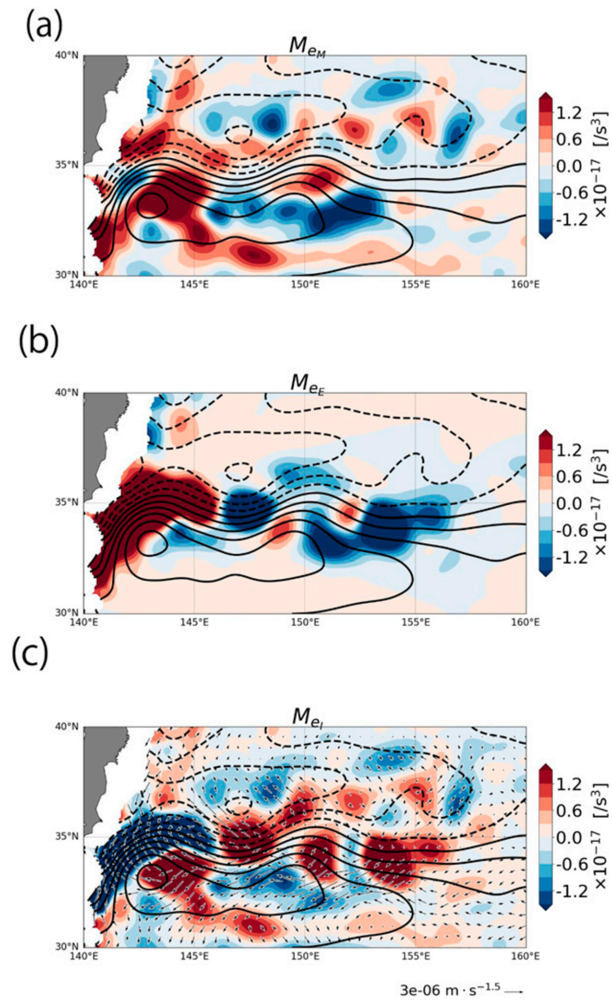

FIG. 10. Horizontal distributions of (a) M_{e_M}, (b) M_{K_E}, and (c) M_{e_I} at a depth of 1342 m. Positive values indicate the mean potential enstrophy loss, the eddy potential enstrophy gain, and the divergence of the interaction potential enstrophy flux, respectively. Black contours in all three panels show the QGPV distribution with the contour interval of $0.5 \times 10^{-5}\,\mathrm{s}^{-1}$. Dashed contours indicate negative QGPV values. Black arrows in (c) indicate the interaction enstrophy flux. The length of the black arrows is drawn to be proportional to the square root of the interaction potential enstrophy flux amplitudes to clearly illustrate weaker fluxes.

5. Summary and conclusions

We have shown the detailed interpretations of terms in the modified Lorentz diagram, especially focusing on the roles played by the interaction energy flux, as a possible diagnostic tool for eddy–mean flow interactions in a limited oceanic region. The barotropic conversion rate in the classical Lorentz diagram considers only a local eddy–mean flow interaction. As documented in Chen et al. (2014, 2016), however, there exist both local and nonlocal eddy–mean flow interactions in the ocean. The energy released from the mean flow is not completely used locally to enhance an eddy field through the barotropic instability process. The remaining energy, once stored in the form of interaction energy, is transported out from the domain in the form of interaction energy flux, and an eddy perturbation field can interact using this interaction energy with the background field in specific regions where the interaction energy flux converges. This suggests that the interaction energy can be considered as a reservoir of nonlocal eddy–mean flow interactions, and as a seed for eddy–mean flow interactions in other regions in a sense. Although the relation to a similar expression using the EP fluxes has already been mentioned in previous studies, we have shown for the first time the relation between the energy diagram and the potential enstrophy diagram, which play complementary roles in understanding eddy–mean flow interactions in the ocean.

The evaluation of each term in the modified energy flux diagram and the potential enstrophy diagram is conducted for the Kuroshio Extension region as an example featuring strong WBC jets. It is found that acceleration of mean flow in the downstream region is partly accomplished by the convergence of interaction energy fluxes. The barotropic conversion rate in the downstream region cannot supply all the kinetic energy gained by the mean flow through eddy–mean flow interaction, and this energy deficit is thus compensated by the interaction energy transported from the upstream region. It is this interaction energy flux that also explains the horizontal distribution of EKE.

The potential enstrophy budget also suggests the mean flow stabilization in the downstream region. One important difference between the energy diagram and the potential enstrophy diagram is the directions of the interaction fluxes. While the interaction energy flux converges in the downstream region, the interaction potential enstrophy flux radiates from the downstream region and converges in the nearshore region. Since the interaction energy flux is related to the Rossby propagation in the idealized case as shown in the appendix, this may be related to the Rossby wave radiation from the EKE maximum near the boundary between the upstream and downstream regions.

Finally, to highlight the advantage in combining different viewpoints for analysis of the eddy–mean flow interactions, the concepts of energy and potential enstrophy diagrams are applied to the NRG in the Kuroshio Extension region. These analyses provide further information about the roles of nonlocal eddy–mean flow interactions, adding to the previous understanding based on momentum and potential vorticity budget (Qiu et al. 2008). While the local energy conversion accelerates the northeastern part of the NRG with the aid of the relatively small nonlocal interaction energy flux convergence, the interaction potential enstrophy flux convergence is crucial around the center of the NRG.

Each method has its own advantages and limitations. They can provide insights from different viewpoints that complement each other. Therefore, the combined use of several methods is required to obtain a comprehensive view of eddy–mean flow interactions, particularly in a limited region.

Acknowledgments. This work was supported by a JSPS Grant-in-Aid for Scientific Research(A) (17H01663) and a JSPS Grant-in-Aid for Transformative Research Areas(B) (20H05731).

APPENDIX

Other Interpretations of the Interaction Energy Flux

Since the interaction energy K_I vanishes in the time-averaged mean, it is not easy to give a physical meaning to the interaction energy flux in a definitive way. Here, the relationship between the energy conversion rate and the Eliassen–Palm fluxes are discussed. We also show two different interpretations of the interaction energy flux divergence M_{K_I}: one by the wave activity conservation law and the other utilizing the total energy conservation law. In this appendix, we drop the reference density ρ_0 from the energy equations and associated conversion rates for simplicity.

a. Link to the Eliassen–Palm fluxes

We introduce the barotropic EP flux vectors (Murakami 2011) to briefly review the relation between M_{K_M} and the EP flux vectors for completeness, and to show a relation between BTR and the Reynolds stress anisotropy. The EP flux concept succeeds in depicting eddy–mean flow interactions such as the standing meanders of the Antarctic Circumpolar Current (Thompson and Garabato 2014) or the blocking events in the Westerlies (Trenberth 1986). The barotropic EP flux vectors shown in Murakami (2011), which are the barotropic version of Trenberth's generalized EP flux vectors (Trenberth 1986), are written as

$$\mathbf{E}_u = \left[\frac{1}{2}(\overline{v'^2} - \overline{u'^2}), -\overline{u'v'}\right], \tag{A1}$$

$$\mathbf{E}_v = \left[-\overline{u'v'}, -\frac{1}{2}(\overline{v'^2} - \overline{u'^2})\right]. \tag{A2}$$

Using these expressions of the EP flux, M_{K_M} can be rewritten as

$$M_{K_M} = -(\overline{u}\nabla_h \cdot \mathbf{E}_u + \overline{v}\nabla_h \cdot \mathbf{E}_v) + \overline{\mathbf{u}_h} \cdot \nabla_h K_E. \tag{A3}$$

Hereafter, we denote the first group of two terms in parentheses on the right-hand side, $-(\overline{u}\nabla_h \mathbf{E}_u + \overline{v}\nabla_h \mathbf{E}_v)$, as M_{EP}, and the last term of the right-hand side, $\overline{\mathbf{u}_h} \cdot \nabla_h K_E$, as M_{EKE}. While there are several definitions for the EP flux (e.g., Plumb 1985a; Trenberth 1986; Thompson and Garabato 2014), the barotropic EP flux vectors in the form of (A1) and (A2) are helpful to interpret the energy conversion rate. This definition of EP flux corresponds to the anisotropic part of the Reynolds stress and M_{EP} can be considered as the work done by the EP flux. On the other hand, M_{EKE} is related to an isotropic part of the Reynolds stress. Since the EKE does not change the mean PV, the influence of the EKE term on the mean flow is often neglected as noneffective forcing in the transformed Eulerian mean (TEM) framework (e.g., Waterman and Jayne 2011), while the pressure forcing associated with the EKE contributes to the mean momentum balances (Aoki et al. 2016).

Similarly, M_{K_E} is decomposed into two or three parts as shown below:

$$M_{K_E} = (\mathbf{E}_u \cdot \nabla_h \overline{u} + \mathbf{E}_v \cdot \nabla_h \overline{v}) - K_E \nabla_h \cdot \overline{\mathbf{u}_h}, \tag{A4}$$

$$= R_1 D_1 + R_2 D_2 - K_E \nabla_h \cdot \overline{\mathbf{u}_h}, \tag{A5}$$

where $D_1 = (\partial\overline{u}/\partial x) - (\partial\overline{v}/\partial y)$, $D_2 = (\partial\overline{u}/\partial y) + (\partial\overline{v}/\partial x)$, $R_1 = (1/2)(\overline{v'^2} - \overline{u'^2})$, and $R_2 = -\overline{u'v'}$. Here D_1 and D_2 are values related to the deformation of two-dimensional mean velocity fields (Okubo 1970; Weiss 1991; Holton and Hakim 2013). D_1 is a pure stretching term, by which a square fluid element deforms into a rhombus. Positive (negative) D_1 indicates a flow field condition for which a fluid element tends to be stretched along the x (y) axis. On the other hand, R_1 is related to the anisotropy of eddies (Hoskins et al. 1983; Marshall et al. 2012; Waterman and Hoskins 2013; Waterman and Lilly 2015). Positive R_1, in which eddies tend to have an elongated shape along the y axis [see Waterman and Hoskins (2013) in detail], disturbs the mean flow and causes it to stretch more in the meridional direction than in the zonal direction. Therefore, a positive value of the product of D_1 and R_1 implies the extraction of the kinetic energy from the mean field by weakening the mean flow stretching. Likewise, R_2 indicates a meridional tilting of eddies, and a positive value of R_2 corresponds to an elongation in the forward direction (Waterman and Hoskins 2013). This term, together with the shear of the mean flow D_2, acquires energy from the mean flow through relaxation of the shear in the mean flow. Finally, $\nabla_h \cdot \overline{\mathbf{u}_h}$ in the Eq. (A5) represents the expansion of fluid elements without changing their shapes. Since an isotropic component of Reynolds stress, i.e., EKE, also works to expand eddies, the term $-K_E \nabla_h \cdot \overline{\mathbf{u}_h}$ indicates the expansion of the mean field.

Considering all together the above three terms in the Eq. (A5), M_{K_E} can be considered as an index that quantifies eddy effects on the deformation of background fields. If M_{K_E} is positive (negative), eddies grow (dissipate) while weakening (strengthening) the mean fields. A parameter for anisotropy γ_m was previously defined in Hoskins et al. (1983) as

$$\gamma_m = \frac{\sqrt{0.5^2(\overline{v'^2 - u'^2})^2 + (\overline{u'v'})^2}}{\mathrm{EKE}} = \frac{\sqrt{R_1^2 + R_2^2}}{\mathrm{EKE}}, \tag{A6}$$

but its physical interpretation had not been clearly indicated. The above formulation of M_{K_E} in Eq. (A5) demonstrates that γ_m can be considered as a ratio of the anisotropic Reynolds stress that increases the anisotropy of mean flow to the EKE effect that increases isotropy of mean flow.

Finally, it is worth noting that M_{K_I} is rewritten by the EP flux vectors, except for the noneffective forcing term, as

$$M_{K_I} = \nabla_h \cdot (-\overline{u}\mathbf{E}_u - \overline{v}\mathbf{E}_v - \overline{\mathbf{u}}_h K_E). \tag{A7}$$

In the case of a two-dimensional barotropic flow, the EP flux term $(-\overline{u}\mathbf{E}_u - \overline{v}\mathbf{E}_v)$ is also included in the radiative wave activity flux (Plumb 1986). The wave activity and its time derivative are a measure of wave amplitude and eddy-transient effects, respectively (Andrews et al. 1987). The interaction energy flux, therefore, can be considered as a measure of wave activity emission. If $M_{K_M} \approx$ BTR, i.e., local eddy–mean flow interaction dominates and noneffective eddy forcing can be neglected, the wave activity is steady. Otherwise, the wave activity is modified by the nonlocality of eddy–mean flow interactions (see next section for more detailed discussions).

b. Wave activity conservation (pseudo-momentum)

As a different way to understand the interaction energy flux, we consider the wave activity conservation law for small-amplitude disturbances in the beta-plane quasigeostrophic (QG) system. Although the assumption of small disturbances may not be adequate for the Kuroshio Extension region, it is useful for obtaining the relationship between the interaction energy flux divergence M_{K_I} and the wave activity, which is widely used in atmospheric wave–mean flow interaction theories (Andrews et al. 1987, and references therein). Our calculation mainly follows the procedure shown in Plumb (1986).

The streamfunction for QG flow is represented as $\psi = p/f$, where p is pressure and $f = f_0 + \beta y$ is the Coriolis parameter, and the QG potential vorticity is written as

$$q = \nabla_h^2 \psi + \beta y + \frac{\partial}{\partial z}\frac{f_0^2}{N^2}\frac{\partial \psi}{\partial z}, \tag{A8}$$

where N is the buoyancy frequency and $\nabla_h = (\partial/\partial x, \partial/\partial y)$. Suppose that the eddy perturbation term is small enough, i.e., $q = Q + q'$, where $q' \ll Q$. Then, the linearized potential vorticity equation for QG flow becomes

$$\frac{\partial q'}{\partial t} + U\frac{\partial q'}{\partial x} + V\frac{\partial q'}{\partial y} + u'\frac{\partial Q}{\partial x} + v'\frac{\partial Q}{\partial y} = S', \tag{A9}$$

and the enstrophy equation is derived as

$$\frac{\partial e}{\partial t} + U\frac{\partial e}{\partial x} + V\frac{\partial e}{\partial y} + \overline{u'q'}\frac{\partial Q}{\partial x} + \overline{v'q'}\frac{\partial Q}{\partial y} = \overline{S'q'}, \tag{A10}$$

where $e = (1/2)\overline{q'q'}$ is the eddy potential enstrophy, $\mathbf{U} = (U, V, 0)$ is the background flow, Q is the background potential vorticity, and S' is the nonconservative eddy source of potential vorticity. It is further assumed that the background flow is conservative, i.e., $U(\partial Q/\partial x) + V(\partial Q/\partial y) = 0$, and slowly varies in space, to ensure following relations:

$$\frac{1}{|\nabla_h Q|}\nabla_h(\mathbf{U}e) \approx \nabla_h\left(\frac{\mathbf{U}e}{|\nabla_h Q|}\right), \tag{A11}$$

$$\frac{\frac{\partial Q}{\partial x}}{|\nabla_h Q|}\overline{u'q'} \approx \nabla \frac{\frac{\partial Q}{\partial x}}{|\nabla_h Q|}\begin{bmatrix} \overline{u'v'} \\ \frac{1}{2}\left(\overline{v'v'} - \overline{u'u'} - \frac{g\overline{\rho'\rho'}}{\rho_0 \partial_z \rho_b}\right) \\ \frac{f_0}{\partial_z \rho_b}\overline{v'\rho'} \end{bmatrix} \tag{A12}$$

and

$$\frac{\frac{\partial Q}{\partial y}}{|\nabla_h Q|}\overline{v'q'} \approx \nabla \frac{\frac{\partial Q}{\partial y}}{|\nabla_h Q|}\begin{bmatrix} \frac{1}{2}\left(\overline{v'v'} - \overline{u'u'} - \frac{g\overline{\rho'\rho'}}{\rho_0 \partial_z \rho_b}\right) \\ -\overline{u'v'} \\ \frac{f_0}{\partial_z \rho_b}\overline{v'\rho'} \end{bmatrix} \tag{A13}$$

The relation (A11) means that the variation of background potential vorticity is relatively small compared to the enstrophy variation along the background mean flow. The assumptions (A12) and (A13) indicate that the direction of background potential vorticity gradient does not change abruptly.

Under these assumptions, we can obtain the wave activity conservation equation

$$\frac{\partial A}{\partial t} + \nabla_h \cdot (\mathbf{U}A) + \nabla \cdot \mathbf{M}_R = \frac{\overline{S'q'}}{|\nabla_h Q|}, \tag{A14}$$

where $A = e/|\nabla_h Q|$ is the pseudo-momentum, i.e., the wave activity. The radiative wave activity flux is written as

$$\mathbf{M}_R = \frac{\gamma}{|\mathbf{U}|}\begin{bmatrix} U\left(\frac{1}{2}\overline{v'v'} - \frac{1}{2}\overline{u'u'} + \frac{1}{2}\frac{g\overline{\rho'\rho'}}{\rho_0\partial_z\rho_b}\right) - V(\overline{u'v'}) \\ -U(\overline{u'v'}) - V\left(\frac{1}{2}\overline{v'v'} - \frac{1}{2}\overline{u'u'} - \frac{1}{2}\frac{g\overline{\rho'\rho'}}{\rho_0\partial_z\rho_b}\right) \\ \frac{f_0}{\partial_z\rho_b}(U\overline{v'\rho'} - V\overline{u'\rho'}) \end{bmatrix}, \tag{A15}$$

where $\gamma = 1$ ($\gamma = -1$) if the background flow is pseudo-eastward (pseudo-westward). Here, pseudo-eastward (pseudo-westward) means the background mean flow is perpendicular to $\nabla_h Q$, with the larger Q value on its right (left) hand side, i.e.,

$$\mathbf{n} = \frac{\nabla_h Q}{|\nabla_h Q|} = \frac{\gamma(-V, U)}{|\mathbf{U}|}. \tag{A16}$$

In the almost-plane wave limit (Plumb 1985b), the wave activity flux $\mathbf{M}_R$ is connected to the group velocity theory. If the streamfunction has the wave form

$$\psi' = \psi_0 \sin(kx + ly + mz - \omega t), \tag{A17}$$

the dispersion relation of the Rossby wave is derived as

$$\omega = kU + lV + \frac{\frac{\partial Q}{\partial x}l - \frac{\partial Q}{\partial y}k}{k^2 + l^2 + \frac{f_0^2}{N^2}m^2}. \tag{A18}$$

With this dispersion relation, simple calculation shows

$$\mathbf{M}_R = (\mathbf{c}_g - \mathbf{U})A, \tag{A19}$$

where $\mathbf{c}_g = (\partial\omega/\partial k, \partial\omega/\partial l, \partial\omega/\partial m)$ is the group velocity. Since $A = (1/4)[k^2 + l^2 + (f_0^2/N^2)m^2]^2/|\nabla_h Q|$ is positive definite, $\mathbf{M}_R$ is everywhere parallel to the group velocity relative to the mean flow.

For the barotropic flow case, the $\mathbf{M}_R$ is connected to the interaction energy flux

$$\mathbf{M}_R = -\frac{\gamma}{|\mathbf{U}|}\mathbf{F}^{(\mathrm{EP})}, \tag{A20}$$

where $\mathbf{F}^{(\mathrm{EP})} = -(U\mathbf{E}_u + V\mathbf{E}_v)$ is the EP flux component of the interaction energy flux in the previous section [see Eq. (A7)]. From the relation (A20), the diabatic component of the interaction energy flux is parallel to the wave activity flux, and therefore the interaction energy flux corresponds to the momentum transport of the waves. Moreover, multiplying (A14) by $|\mathbf{U}|$, under the assumption of a slowly varying magnitude of the background velocity compared to that of the wave activity A, gives the modified wave activity equation

$$\frac{\partial \tilde{A}}{\partial t} + \nabla_h \cdot (\mathbf{U}\tilde{A}) + \nabla_h \cdot [-\gamma\mathbf{F}^{(\mathrm{EP})}] = \frac{|\mathbf{U}|\overline{S'q'}}{|\nabla_H Q|}, \tag{A21}$$

where $\tilde{A} = |\mathbf{U}|A$ is the modified wave activity flux. Using (A19), $-\gamma\mathbf{F}^{(\mathrm{EP})}$ is shown to be the radiative flux of the modified wave activity $\tilde{A}$

$$-\gamma\mathbf{F}^{(\mathrm{EP})} = (\mathbf{c}_g - \mathbf{U})\tilde{A}. \tag{A22}$$

Thus, the interaction energy flux neglecting noneffective eddy forcing represents the wave propagation and its momentum transport. If the barotropic eddy–mean flow interaction occurs nonlocally, i.e., $M_{K_M} \neq M_{K_E}$, the wave activity radiates from the parcel flowing along the background field. Therefore, nonlocal eddy–mean flow interactions can be considered as the wave radiation and its momentum transport.

c. *Total energy conservation*

The total kinetic energy conservation can be written as

$$\frac{\partial \mathcal{E}}{\partial t} + \nabla \cdot (\mathbf{F} + \overline{\mathbf{u}}\mathcal{E}) = (\text{forcing}), \tag{A23}$$

where $\mathcal{E} = (K_M + K_E)$ is the total energy, and

$$\begin{aligned}\mathbf{F} &= \left[\overline{\mathbf{u}'\frac{1}{2}(u'^2 + v'^2)}\right] + (\overline{\mathbf{u}}\,\overline{p} + \overline{\mathbf{u}'p'}) + \rho_0(\overline{u}\,\overline{u'\mathbf{u}'} + \overline{v}\,\overline{v'\mathbf{u}'}) \\ &= \mathbf{F}_{\mathrm{eddy}} + \overline{\mathbf{u}p} + \mathbf{F}_I \end{aligned} \tag{A24}$$

is the energy flux that consists of the eddy–eddy interaction energy flux $\mathbf{F}_{\mathrm{eddy}}$, the pressure work $\overline{\mathbf{u}p}$, and the eddy–mean flow interaction flux $\mathbf{F}_I$. The energy equation takes the form of a conservation equation, where the total (i.e., radiative plus advective) energy flux $\mathbf{F} + \overline{\mathbf{u}}\mathcal{E}$ represents the local energy transport. The influence of eddy–mean flow interaction in this energy transport appears only in the $\mathbf{F}_I$ term, except for the advection terms. The horizontal divergence of the interaction flux, $\nabla \cdot \mathbf{F}_I$, corresponds to the interaction energy flux divergence M_{K_I} in the main text (see section 2a). Note that if energy conversion only occurs locally, i.e., $M_{K_I} = 0$, the convergence of interaction energy flux is also zero, i.e., $\nabla \cdot \mathbf{F}_I = 0$, and therefore, eddy–mean flow interaction does not affect the total energy distribution. This indicates that the interaction energy flux divergence appearing in the modified Lorentz diagram represents the transport of total energy due to the nonlocality of eddy–mean flow interaction. In this sense, we may call M_{K_I} the *energy flux divergence of the eddy–mean flow interaction* instead of the interaction energy flux divergence.

REFERENCES

Andrews, D., C. Leovy, and J. Holton, 1987: *Middle Atmosphere Dynamics*. Academic Press, 489 pp.

Andrews, D. G., 1983: A conservation law for small-amplitude quasi-geostrophic disturbances on a zonally asymmetric basic flow. *J. Atmos. Sci.*, **40**, 85–90, https://doi.org/10.1175/1520-0469(1983)040<0085:ACLFSA>2.0.CO;2.

Aoki, K., A. Kubokawa, R. Furue, and H. Sasaki, 2016: Influence of eddy momentum fluxes on the mean flow of the Kuroshio Extension in a 1/10° ocean general circulation model. *J. Phys. Oceanogr.*, **46**, 2769–2784, https://doi.org/10.1175/JPO-D-16-0021.1.

Chelton, D. B., M. G. Schlax, and R. M. Samelson, 2011: Global observations of nonlinear mesoscale eddies. *Prog. Oceanogr.*, **91**, 167–216, https://doi.org/10.1016/j.pocean.2011.01.002.

Chen, R., G. R. Flierl, and C. Wunsch, 2014: A description of local and nonlocal eddy–mean flow interaction in a global eddy-permitting state estimate. *J. Phys. Oceanogr.*, **44**, 2336–2352, https://doi.org/10.1175/JPO-D-14-0009.1.

——, A. F. Thompson, and G. R. Flierl, 2016: Time-dependent eddy–mean energy diagrams and their application to the ocean. *J. Phys. Oceanogr.*, **46**, 2827–2850, https://doi.org/10.1175/JPO-D-16-0012.1.

Greatbatch, R. J., X. Zhai, M. Claus, L. Czeschel, and W. Rath, 2010: Transport driven by eddy momentum fluxes in the Gulf Stream Extension region. *Geophys. Res. Lett.*, **37**, L24401, https://doi.org/10.1029/2010GL045473.

Holton, J., and G. Hakim, 2013: *An Introduction to Dynamic Meteorology*. Elsevier, 552 pp.

Hoskins, B. J., I. N. James, and G. H. White, 1983: The shape, propagation and mean-flow interaction of large-scale weather systems. *J. Atmos. Sci.*, **40**, 1595–1612, https://doi.org/10.1175/1520-0469(1983)040<1595:TSPAMF>2.0.CO;2.

Lorentz, E. N., 1955: Available potential energy and the maintenance of the general circulation. *Tellus*, **7**, 157–167, https://doi.org/10.1111/j.2153-3490.1955.tb01148.x.

Magalhães, F. C., J. L. L. Azevedo, and L. R. Oliveira, 2017: Energetics of eddy-mean flow interactions in the Brazil current between 20°S and 36°S. *J. Geophys. Res. Oceans*, **122**, 6129–6146, https://doi.org/10.1002/2016JC012609.

Marshall, D. P., J. R. Maddison, and P. S. Berloff, 2012: A framework for parameterizing eddy potential vorticity fluxes. *J. Phys. Oceanogr.*, **42**, 539–557, https://doi.org/10.1175/JPO-D-11-048.1.

Masumoto, Y., 2010: Sharing the results of a high-resolution ocean general circulation model under a multi-discipline framework—A review of OFES activities. *Ocean Dyn.*, **60**, 633–652, https://doi.org/10.1007/s10236-010-0297-z.

——, and Coauthors, 2004: A fifty-year eddy-resolving simulation of the world ocean: Preliminary outcomes of OFES (OGCM for the Earth Simulator). *J. Earth Simul.*, **1**, 35–56.

Murakami, S., 2011: Atmospheric local energetics and energy interactions between mean and eddy fields. Part I: Theory. *J. Atmos. Sci.*, **68**, 760–768, https://doi.org/10.1175/2010JAS3664.1.

Nakamura, M., and Y. Chao, 2001: Diagnoses of an eddy-resolving Atlantic Ocean model simulation in the vicinity of the Gulf Stream. Part I: Potential vorticity. *J. Phys. Oceanogr.*, **31**, 353–378, https://doi.org/10.1175/1520-0485(2001)031<0353:DOAERA>2.0.CO;2.

Ogata, T., and Y. Masumoto, 2011: Interannual modulation and its dynamics of the mesoscale eddy variability in the southeastern tropical Indian Ocean. *J. Geophys. Res.*, **116**, C05005, https://doi.org/10.1029/2010JC006490.

Okubo, A., 1970: Horizontal dispersion of floatable particles in the vicinity of velocity singularities such as convergences. *Deep-Sea Res. Oceanogr. Abstr.*, **17**, 445–454, https://doi.org/10.1016/0011-7471(70)90059-8.

Pacanowski, R. C., and S. M. Griffies, 2000: MOM 3.0 Manual. NOAA Geophysical Fluid Dynamic Laboratory, 682 pp.

Plumb, R. A., 1983: A new look at the energy cycle. *J. Atmos. Sci.*, **40**, 1669–1688, https://doi.org/10.1175/1520-0469(1983)040<1669:ANLATE>2.0.CO;2.

——, 1985a: An alternative form of Andrews' Conservation Law for quasi- geostrophic waves on a steady, nonuniform flow. *J. Atmos. Sci.*, **42**, 298–300, https://doi.org/10.1175/1520-0469(1985)042<0298:AAFOAC>2.0.CO;2.

——, 1985b: On the three-dimensional propagation of stationary waves. *J. Atmos. Sci.*, **42**, 217–229, https://doi.org/10.1175/1520-0469(1985)042<0217:OTTDPO>2.0.CO;2.

——, 1986: Three-dimensional propagation of transient quasi-geostrophic eddies and its relationship with the eddy forcing of the time-mean flow. *J. Atmos. Sci.*, **43**, 1657–1678, https://doi.org/10.1175/1520-0469(1986)043<1657:TDPOTQ>2.0.CO;2.

Qiu, B., and S. Chen, 2010: Eddy-mean flow interaction in the decadally modulating Kuroshio Extension system. *Deep. Sea Res. II*, **57**, 1098–1110, https://doi.org/10.1016/j.dsr2.2008.11.036.

——, ——, P. Hacker, N. G. Hogg, S. R. Jayne, and H. Sasaki, 2008: The Kuroshio Extension northern recirculation gyre: Profiling float measurements and forcing mechanism. *J. Phys. Oceanogr.*, **38**, 1764–1779, https://doi.org/10.1175/2008JPO3921.1.

Rhines, P. B., and W. R. Holland, 1979: A theoretical discussion of eddy-driven mean flows. *Dyn. Atmos. Oceans*, **3**, 289–325, https://doi.org/10.1016/0377-0265(79)90015-0.

Sasaki, H., Y. Sasai, M. Nonaka, Y. Masumoto, and S. Kawahara, 2006: An eddy-resolving simulation of the quasi-global ocean driven by satellite-observed wind field preliminary outcomes from physical and biological fields. *J. Earth Simul.*, **6**, 35–49.

——, M. Nonaka, Y. Masumoto, Y. Sasai, H. Uehara, and H. Sakuma, 2008: An eddy-resolving hindcast simulation of the quasiglobal ocean from 1950 to 2003 on the Earth Simulator. *High Resolution Numerical Modelling of the Atmosphere and Ocean*, K. Hamilton, and W. Ohfuchi, Eds., Springer, 157–185.

Takaya, K., and H. Nakamura, 2001: A formulation of a phase-independent wave-activity flux for stationary and migratory quasigeostrophic eddies on a zonally varying basic flow. *J. Atmos. Sci.*, **58**, 608–627, https://doi.org/10.1175/1520-0469(2001)058<0608:AFOAPI>2.0.CO;2.

Thompson, A. F., and A. C. N. Garabato, 2014: Equilibration of the Antarctic Circumpolar Current by standing meanders. *J. Phys. Oceanogr.*, **44**, 1811–1828, https://doi.org/10.1175/JPO-D-13-0163.1.

Trenberth, K. E., 1986: An assessment of the impact of transient eddies on the zonal flow during a blocking episode using localized Eliassen–Palm flux diagnostics. *J. Atmos. Sci.*, **43**, 2070–2087, https://doi.org/10.1175/1520-0469(1986)043<2070:AAOTIO>2.0.CO;2.

Wang, M., Y. Du, B. Qiu, X. Cheng, Y. Luo, X. Chen, and M. Feng, 2017: Mechanism of seasonal eddy kinetic energy variability in the eastern equatorial Pacific Ocean. *J. Geophys. Res. Oceans*, **122**, 3240–3252, https://doi.org/10.1002/2017JC012711.

Waterman, S., and S. R. Jayne, 2011: Eddy–mean flow interactions in the along-stream development of a western boundary current jet: An idealized model study. *J. Phys. Oceanogr.*, **41**, 682–707, https://doi.org/10.1175/2010JPO4477.1.

——, and B. J. Hoskins, 2013: Eddy shape, orientation, propagation, and mean flow feedback in western boundary current jets. *J. Phys. Oceanogr.*, **43**, 1666–1690, https://doi.org/10.1175/JPO-D-12-0152.1.

——, and J. M. Lilly, 2015: Geometric decomposition of eddy feedbacks in barotropic systems. *J. Phys. Oceanogr.*, **45**, 1009–1024, https://doi.org/10.1175/JPO-D-14-0177.1.

Weiss, J., 1991: The dynamics of enstrophy transfer in two-dimensional hydrodynamics. *Physica D*, **48**, 273–294, https://doi.org/10.1016/0167-2789(91)90088-Q.